CrystEngComm

Accepted Manuscript

ROYAL SOCIETY OF CHEMISTRY

www.rsc.org/crystengcomm

Highly pH-dependent synthesis of two novel three-dimensional dysprosium complexes with interesting magnetic and luminescent properties†

Lina Zhang,[a,b] Shuting Lu,[a] Chao Zhang,[a] Chenxia Du,*[a] and Hongwei Hou*[a]

[a] *College of Chemistry and Molecular Engineering, Zhengzhou University, Zhengzhou, 450052, P.R. China.*

[b] *College of Physics and Chemistry, Henan Polytechnic University, Jiaozuo 454003, P. R. China.*

E-mail: dcx@zzu.edu.cn, houhongw@zzu.edu.cn.

Abstract: Two novel Dy-based MOFs, namely, $\{[Dy_2(PA)_3(H_2O)_3(DMF)]\cdot(DMF)_2\cdot(H_2O)\}_n$ (**1**) and $\{[Dy_2(PA)_3(H_2O)_2(DMF)_2]\cdot(DMF)_3\cdot(H_2O)\}_n$ (**2**) (H_2PA = pamoic acid) were solvothermally synthesized from the reaction of $Dy(NO_3)_3$ and H_2PA under different pH values. Interestingly, both the complexes can be obtained simultaneously within the pH range of 5.0-6.2, while higher pH values (6.2-7.0) promote the formation of compound **1**, and lower pH values (2.0-5.0) prefer to produce pure complex **2**. Single-crystal X-ray diffraction studies indicate that **1** and **2** are both three-dimensional frameworks composed of dinuclear Dy(III) subunits featuring **pcu** networks with the point symbol of $\{4^{12}\cdot6^3\}$. Significantly, slight structure difference makes these two compounds showing completely different magnetic properties. Variable temperature magnetization measurements ($\chi_M T$-T) demonstrate ferromagnetic interactions in compound **1**, while possible antiferromagnetic interactions were observed in compound **2**. Alternating-current (ac) susceptibility measurements indicate that both in-phase (χ') and out-of-phase (χ'') components showed frequency dependence in compound **1**, suggesting that there is a slow relaxation behavior of the magnetization, which is typical of single-molecule magnets (SMMs), while no out-of-phase ac signal is noticed for **2**. Furthermore, both **1** and **2** exhibit characteristic luminescence of Dy^{3+} upon excitation at 365 nm, but with different intensities. The reasons causing such magnetic and luminescent differences are discussed in detail.

Introduction

Single-molecule magnets (SMMs) have currently been a fertile topic of research owing to their slow magnetic relaxation features that are potentially suitable for applications in high-density information storage, quantum computing devices, and spintronics.[1] Lanthanide elements, in particular the Dy^{3+} ion, seem to be extremely useful in this respect, benefiting from both the large magnetic moments and strong anisotropy. [2] Indeed, a large number of researches have been carried out on Dy-based SMMs, some of which show impressive SMM properties, such as high energy barriers (U_{eff}) and/or blocking temperatures (T_B). [3-12] Compared with the 3d metal based SMMs, the magnetic relaxation in polynuclear Ln systems is more difficult to elucidate due to several factors, such as large magnetic anisotropy of the Ln^{3+} ions, high tunneling rates, and the weak magnetic interactions between the Ln^{3+} ions.[8b]

Recently, considerable efforts have been devoted to regulating the magnetic behaviours by tuning molecular structures. A fascinating instance among such researches was the observation of adjustable SMM properties in complexes $[Dy_2(phen)_2(L)_6]\cdot2H_2O$ and $[Dy_2(phen)_2(L)_6]$, [4a] which was associated with the changes of the coordination environment of Dy^{3+} ions originating from the dehydration of the terminal coordinated water molecules. More recently, Sessoli and co-workers demonstrated that the magnetic anisotropy of $[Na\{Dy(DOTA)(H_2O)\}]\cdot4H_2O$ (DyDOTA) is largely influenced by the orientation of the apical water molecule. [9, 12b] Most of these instances demonstrate that even subtle structural changes could affect the orientation of the magnetization easy-axis of the lanthanide ion, [13, 15, 16, 19-23] and lead to different dynamic magnetic behaviors. [24-26]

It is well known that pH conditions have a

significant influence on the construction of structurally diverse MOFs, and the most frequently observed effects caused by changing pH values are the different dimension of the resulting metal-organic architectures, especially for the transition metal ions. [27] In this work, we focus our interest on preparing Dy-based SMMs under different pH conditions and investigating the magneto–structural correlations in these dysprosium complexes. We expect that different pH conditions of the starting materials may create Dy-MOFs with distinct coordination environments, and then different magnetic anisotropy and SMM properties could be achieved. In this paper, we purposefully choose pamoic acid [28-30] (4,4′-methylenebis[3-hydroxy-2-naphthalenecarboxylic acid], Scheme 1) as a bridging ligand to construct dysprosium complexes based on the following considerations: (i) it possesses both carboxylic and phenol hydroxyl groups which have the tendency to be completely or partially deprotonated, producing various acidity-dependent coordination modes; (ii) its multifunctional coordination sites and strong coordinate ability with lanthanide ions may generate unusual structures with promising properties; (iii) so far, only two lanthanide complexes based on pamoic acid have been reported, [31] and no systematic investigation concerning the magneto–structural correlations and the effect of acidity on the construction of Ln-MOFs based on pamoic acid has been carried out.

Herein, two novel Dy-based MOFs $\{[Dy_2(PA)_3(H_2O)_3(DMF)]\cdot(DMF)_2\cdot(H_2O)\}_n$ (**1**) and $\{[Dy_2(PA)_3(H_2O)_2(DMF)_2]\cdot(DMF)_3\cdot(H_2O)\}_n$ (**2**) (H_2PA = pamoic acid) were solvothermally synthesized from the reaction of $Dy(NO_3)_3$ and pamoic acid under different pH values. Interestingly, both the complexes can be obtained simultaneously within the pH range of 5.0-6.2, while higher pH values (6.2-7.0) promote the formation of single-phase dysprosium compound **1**, and lower pH values (2.0-5.0) prefer to produce pure complex **2**. Variable temperature magnetization measurements ($\chi_M T$–T), field-dependent magnetization measurements $M(H)$, and alternating current (ac) susceptibility measurements were performed in detail. In addition, luminescent properties of complexes **1** and **2** were also investigated. The reasons causing magnetic and luminescent differences are discussed thoroughly.

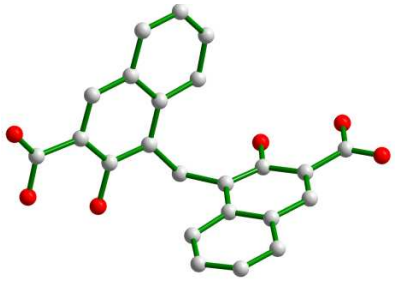

Scheme 1 Representation of pamoic acid. Colour code: O, red; C, grey. The H atoms have been omitted for clarity.

Experimental section

Materials and physical measurements

All reagents and solvents employed were commercially available and used as received without further purification. Elemental analyses (C, H, and N) were carried out on a Flash EA 1112 elemental analyzer. IR data were recorded on a BRUKER TENSOR 27 spectrophotometer with KBr pellets in the region of 400−4000 cm^{-1}. Powder X-ray diffraction (PXRD) patterns were recorded using Cu Kα radiation (λ = 1.5406 Å) on a PANalytical X'Pert PRO diffractometer. Thermogravimetric analysis (TGA) experiments were performed on a Netzsch STA 449C thermal analyzer at a heating rate of 10 °C/min in air. All magnetization data were recorded on a Quantum Design MPMS-XL-7 SQUID magnetometer. The variable-temperature magnetization was measured with an external magnetic field of 1000 Oe in the temperature range 2–300 K. Absorption spectra were measured on a Perkin-Elmer Lambda 900 spectrometer at room temperature. The emission spectra of the Dy(III) complexes in solid state were recorded at an angle of 22.5° (front face) on a HORIBA JOBIN YVON FluoroMax-P spectrophotometer equipped with both continuous and pulsed xenon lamps.

Synthesis of the compounds

$\{[Dy_2(PA)_3(H_2O)_3(DMF)]\cdot(DMF)_2\cdot(H_2O)\}_n$ (1) A mixture of $Dy(NO_3)_3\cdot 6H_2O$ (45.6 mg, 0.1 mmol), H_2PA

(38.8 mg, 0.1 mmol), DMF (4 mL) and distilled H_2O (6 mL) was placed in a 25 mL beaker. The pH value of the mixture was adjusted to 6.2-7.0 with 0.5 mol·L^{-1} sodium hydroxide aqueous solution. After stirring for 0.5 h at room temperature, the mixture was sealed in the Teflon-lined stainless steel vessel and heated at 110 °C for three days under autogenous pressure. The vessel was then cooled slowly down to room temperature at 5 °C/h, deep yellow prismatic crystals of **1** were produced (yield, 45% based on Dy). Anal. Calcd for $C_{78}H_{71}Dy_2N_3O_{25}$: C, 52.72; H, 4.00; N, 2.37%. Found: C, 53.31; H, 3.98; N, 2.32%. IR (KBr, cm^{-1}): 3422 (b), 3061(w), 2933(w), 1648(vs), 1537(w), 1457(m), 1398(s), 1233(w), 1093(w), 810(w), 751.3(w).

$\{[Dy_2(PA)_3(H_2O)_2(DMF)_2]\cdot(DMF)_3\cdot(H_2O)\}_n$ (2) Pale yellow plate-shaped crystals of **2** can be obtained following the same synthetic procedures as that of **1** except that the pH value was adjusted to 2.0-5.0 by 0.5 mol·L^{-1} hydrochloric acid aqueous solution. Yield ca. 43%. Anal. Calcd for $C_{84}H_{83}Dy_2N_5O_{26}$: C, 52.95; H, 4.36; N, 3.68%. Found: C, 53.42; H, 4.37; N, 3.68%. IR (KBr, cm^{-1}): 3417(b), 3057(w), 2928(w), 1646(vs), 1458(m), 1395(s), 1203(w), 1097(w), 813(w), 748(w).

Notably, when the reaction was carried out at the initial pH value of 5.4 without regulating the acidity of the mixture, both **1** and **2** were obtained simultaneously. Further studies indicate that both the compounds can also be generated simultaneously within the pH range of 5.0-6.2.

Crystal data collection and refinement

Single-crystal structure determination of compounds **1** and **2** were carried out on an Oxford Diffraction Xcalibur CCD diffractometer with graphite-monochromated Mo-$K\alpha$ radiation (λ = 0.71073Å) at 291 K using the ω-scan technique. The structures were obtained by the direct methods using the program SHELXS-97 and all non-hydrogen atoms were refined anisotropically on F^2 by the full-matrix least-squares technique which used the SHELXL-97 crystallographic software package.[32] The hydrogen atoms were included in the structure factor calculation at idealized positions by using a riding model. The crystal data, data collection and refinement parameters for **1** and **2** are listed in Table 1. The Flack parameter of compound **2** is also listed in Table 1. Because the "twin" refinement was used with a BASF value of 0.55352, compound **2** turns out to be a racemic twin structure. CCDC reference numbers for **1** and **2** are 997901 and 997902, respectively.

Table 1. Crystallographic data and structural refinement summary for compounds **1**−**2**

	1	**2**
Empirical formula	$C_{78}H_{71}Dy_2N_3O_{25}$	$C_{84}H_{83}Dy_2N_5O_{26}$
Formula weight	1775.36	1903.54
T (K)	291.15	291.15
crystal system	monoclinic	orthorhombic
space group	$P2_1/c$	$Pna2_1$
a(Å)	14.06551(16),	19.1237(3)
b(Å)	29.3960(3),	14.4603(2)
c(Å)	18.4286(3)	30.6247(4)
α(°)	90.00	90.00
β(°)	107.0581(14)	90.00
γ(°)	90.00	90.00
V(Å^3)	7284.48(15)	8468.8(2)
Z	4	4
D_{calcd} [g /cm^3]	1.617	1.491
μ(mm^{-1})	2.120	1.831
F(000)	3560	3840.0
Reflections collected	31911	24916
Unique reflections	15311	14672
Goodness-of-fit	1.090	1.053
R_1[a] ($I>2\sigma(I)$)	0.0383	0.0388
wR_2[b] (all data)	0.0931	0.0974
R(int)	0.0283	0.0302
Flack parameter		0.00(8)

[a] $R_1=\Sigma||Fo|-|Fc||/\Sigma|Fo|$. [b] $wR_2=[\Sigma[w(Fo^2-Fc^2)^2]/\Sigma w(Fo^2)^2]^{1/2}$

Results and discussion

Synthesis and characterization

Solvothermal reaction is preference to the other methods in this system because of the limited solubility of pamoic acid. It is surprisingly to find that both compounds **1** and **2** were obtained simultaneously when the reaction was carried out for three days at an initial pH value of 5.4. Systematic investigations concerning the effect of acidity on the construction of the resultant crystals were carried out. With the increase of pH values from 5.4 to 6.2 by adding 0.5 mol/L sodium hydroxide aqueous solution, more complex **1** and less complex **2** were generated simultaneously. When the pH was above

6.2, only crystals of complex **1** and a little yellow precipitates were obtained, while only yellow precipitates were produced at pH above 7.0. On the other hand, when we regulated the pH of the starting materials to the range of 5.0−2.0 with 0.5 mol·L^{-1} hydrochloric acid aqueous solution, only crystals of complex **2** and some precipitates were produced, while only precipitates were obtained when the pH is less than 2.0. The above results demonstrate that pH conditions of the mixture played a significant role in synthesizing and separating the resultant crystal samples. Both compounds can be obtained simultaneously within the pH range of 5.0-6.2, and single-phase **1** and **2** can be generated separately by regulating the reaction pH values to 6.2-7.0 and 5.0-2.0. Actually, the subtle changes in the coordination modes of H_2PA at different pH conditions result in such two MOFs with distinct structures.[28b] In the IR Spectra of the complexes, the broad absorption bands in the range of 3500−3410 cm^{-1} indicate the presence of water molecules in the structures. The absence of characteristic absorption of ν_{as}(COOH) near 1700 cm^{-1} indicates that pamoic acid is completely deprotoned in both complexes. [31] The ν_{as}(COO^-) vibration of the carboxylate group occurs at 1648 and 1646 cm^{-1} for **1** and **2**, respectively, while those of ν_s(COO^-) occur at 1398 and 1395 cm^{-1}, respectively. The large difference in the $\Delta(\nu_{as}-\nu_s)$ values of 250 cm^{-1} for **1** and 251 cm^{-1} for **2** evidence the presence of both chelating bidentate and bis-monodentate mode of pamoic acid (Scheme 2).

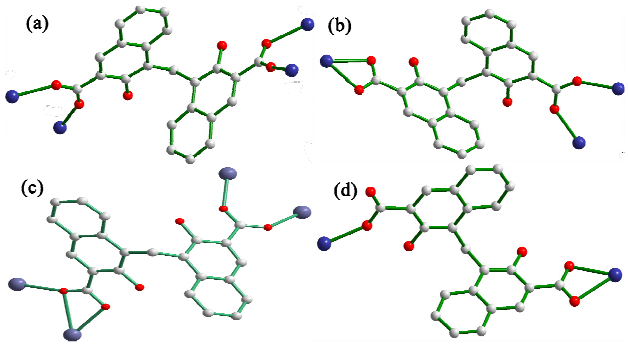

Scheme 2. Coordination modes of the ligand PA^{2-} found in compounds **1** (a, b) and **2** (c, d).

Description of the crystal structures

$\{[Dy_2(PA)_3(H_2O)_3(DMF)]\cdot(DMF)_2\cdot(H_2O)\}_n$ (1) Single-crystal X-ray structural analysis reveals that compound **1** crystallizes in monoclinic space group $P2_1/c$. The asymmetric unit of **1** contains two crystallographically independent Dy^{III} ions, three PA^{2-} anions, three coordinated water molecules, one coordinated DMF molecule, two free DMF and about one free water molecules (Fig. 1a). Details of the crystal parameters, structure refinement and selected bond lengths and angles are listed in Table 1 and Table S1 (ESI†), respectively. As depicted in Fig. 1b, it contains the dinuclear core of $[Dy_2(COO)_6(H_2O)_3(DMF)]$ as the secondary building unit (SBU). Each SBU consists of two eight-coordinated Dy^{3+} ions and six $-COO^-$ groups. Four of the $-COO^-$ groups bridge the two Dy^{3+} centers in a μ_2 : η^1: η^1 fashion. The remaining two $-COO^-$ groups act as chelating ligands, with each of them coordinating to a single Dy^{3+} ion. Two H_2O molecules coordinate with Dy1 center while Dy2 center is coordinated with one H_2O and one DMF molecules (Fig. 1b). It is interesting to note that although two hydroxy groups are located in the *ortho*-position to the carboxylate groups in the pamoic acid, each of them was uncoordinated. The Dy–O bond lengths are in the range of 2.286(2)–2.488(2) and 2.314(2)–2.476(3) Å for Dy1 and Dy2 centers, respectively, comparable to those of other dysprosium–oxygen compounds.[4a,14] The coordination geometry around Dy1 center can be described as a distorted triangular dodecahedron, while that of Dy2 center can be described as a distorted bicapped trigonal prism (Fig. 2). Remarkably, each SBU of compound **1** is connected to six nearby SBUs through PA^{2-} anions forming a fascinating "snowflake" configuration (Fig. 3), which are further linked by PA^{2-} anions to furnish a porous 3D framework (Fig. 4a). The Dy···Dy distance in the dinuclear unit of compound **1** is 4.3721(0) Å, while the shortest Dy···Dy distance between adjacent SBUs is 6.6805(1) Å.

Topological analysis has been applied for better understanding the connectivity of 3D framework in

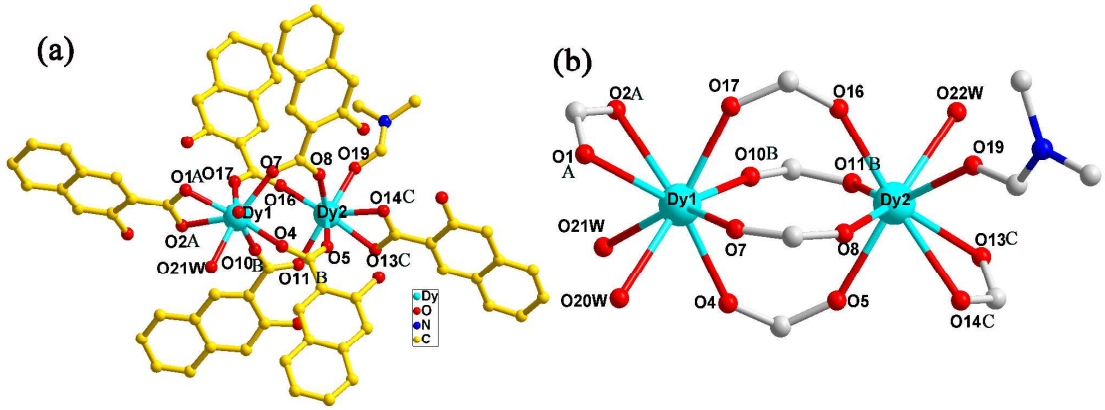

Fig. 1 (a) Local coordination environments of Dy^{III} centers in **1**. All hydrogen atoms and lattice DMF molecule are omitted for clarity. (b) Representations of the dinuclear SBU of compound **1**. Symmetry code, A: -X, 1/2+Y, 1/2-Z; B: -1+X, 1/2-Y, -1/2+Z; C: 1-X, -1/2+Y, 1/2-Z.

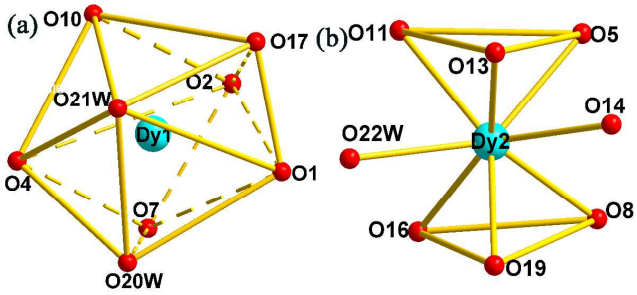

Fig. 2 The coordination geometries of Dy1 and Dy2 centers in compound **1**.

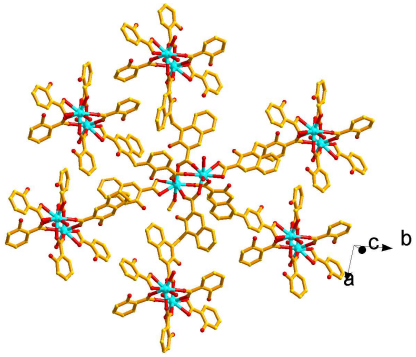

Fig. 3 Views representing the connection of each SBU to six nearby SBUs though PA^{2-} anions in **1**, showing a "snowflake" configuration.

compound **1**. The binuclear unit $[Dy_2(COO)_6(H_2O)_3(DMF)]$ as a SBU is connected to six adjacent dysprosium dimers by six PA^{2-} anions, forming a 6-connected node. The PA^{2-} anions act as linear bridges between the binuclear unit nodes. Such connectivity repeats infinitely, resulting in a 3D **pcu** network, with the point symbol of $\{4^{12}\cdot6^3\}$. The topology is shown in Fig. 4b.

$\{[Dy_2(PA)_3(H_2O)_2(DMF)_2]\cdot(DMF)_3\cdot(H_2O)\}_n$ **(2)**

Compound **2** crystallizes in orthorhombic space group $Pna2_1$. The asymmetric unit of **2** contains two crystallographically independent Dy^{III} ions, three PA^{2-} anions, two coordinated DMF molecules, two coordinated water molecules, three lattice DMF molecules and about one lattice water molecule (Fig. 5a). Its structure is similar to **1** with a dinuclear core of $[Dy_2(COO)_6(DMF)_2(H_2O)_2]$ as the secondary building unit (Fig. 5b). A closer look at the structures of both compounds reveals the differences. Firstly, four carboxyl groups of **2** bridge the two Dy^{3+} centers in both $\mu_2:\eta^1:\eta^1$ and $\mu_2:\eta^1:\eta^2$ fashions, whereas only $\mu_2:\eta^1:\eta^1$ coordination mode exists in **1**. Secondly, one of the remaining two $-COO^-$ groups coordinates with a single Dy^{3+} ion as a mono-dentate ligand in **2**, while two of the $-COO^-$ groups act as chelating ligands in **1**. Furthermore, in the dinuclear core of **1**, only Dy2 center is coordinated with one DMF molecule, while in **2**, each Dy^{3+} center is coordinated by one DMF molecule. The Dy–O bond distances of **2** are in the range of 2.343(3)–2.454(3) Å and 2.269(3)–2.676(3) Å for Dy1 and Dy2 centers, respectively, comparable to those of other dysprosium–oxygen compounds. [14] The coordination geometry around Dy1 center can be described as a distorted bicapped trigonal prism, while that of Dy2 center can be described as a distorted triangular dodecahedron (Fig. 6). The Dy···Dy distance in the dinuclear unit of **2** is 4.0045(1)

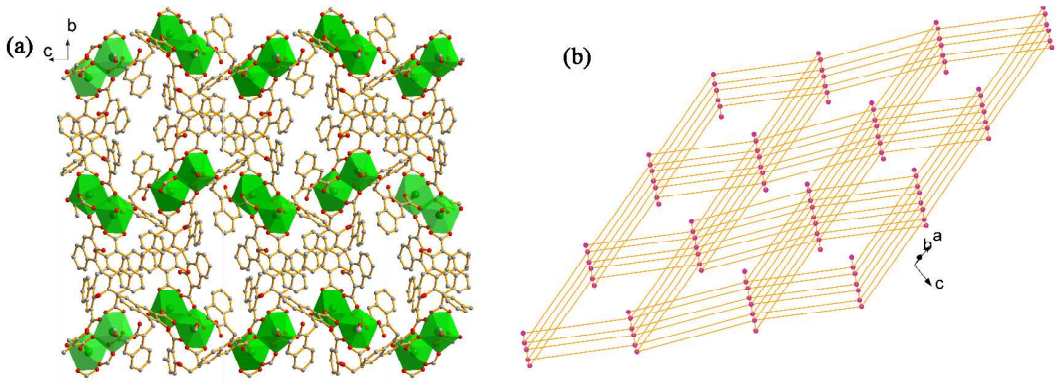

Fig. 4 (a) Three-dimensional porous structure of compound **1**. (b) Schematic topological view of the 3D structure of $\{4^{12}\cdot6^3\}$ topology in **1**. (Color code: $[Dy_2(COO)_6(H_2O)_3(DMF)]$, violet ball; PA^{2-} anion, orange line.)

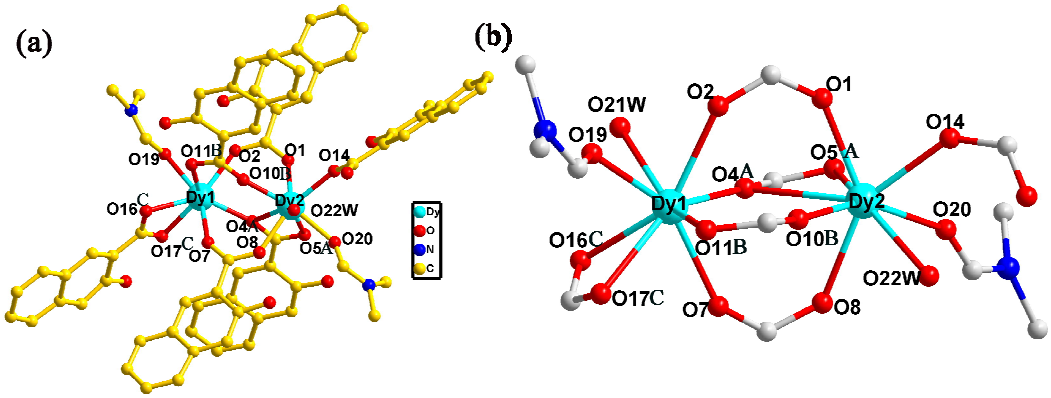

Fig. 5 (a) Local coordination environments of Dy^{III} centers in **2**. All hydrogen atoms and lattice DMF molecule are omitted for clarity. (b) Representations of the dinuclear SBU of compound **2**. Symmetry code, A: -1/2+X, 3/2-Y, +Z; B: 1/2+X, 1/2-Y, +Z; C: 1/2-X, -1/2+Y, 1/2+Z.

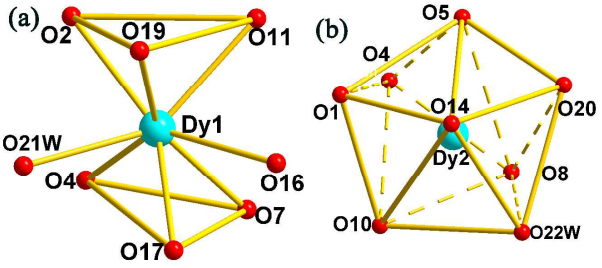

Fig. 6 The coordination geometries of Dy1 and Dy2 centers in compound **2**.

Å, which is a little shorter than that in **1**. The shortest Dy···Dy distance between adjacent SBUs is 11.3725(1) Å for **2**, which is much longer than that in**1**. Each SBU of compound **2** is connected to six nearby SBUs through the PA^{2-} anions forming an interesing configuration along the *c* axis (Fig. 7). These SBUs are further linked by PA^{2-} anions producing a porous 3D network (Fig. 8a). Notably, 1D rhombus channels with window sizes of 13.5 × 13.5 $Å^2$ (excluding van der Waals radii of the atoms) exist in **2** along the *a* axis (Fig. 8a). The solvent-accessible volume of compound **2** calculated by PLATON[37] is 2767.9 $Å^3$ corresponding to 32.7% of the unit cell volume. Lattice DMF solvent molecules are filled in these channels (Fig. 8b).

Topological analysis has been applied for better understanding the connectivity of the framework in compound **2**, and a 3D **pcu** network with the point symbol of $\{4^{12}\cdot6^3\}$ is observed. The topology is shown in Fig. 9.

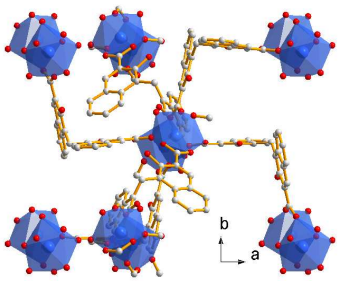

Fig. 7 Views representing the connection of each SBU to six nearby SBUs though PA^{2-} anions in **2**.

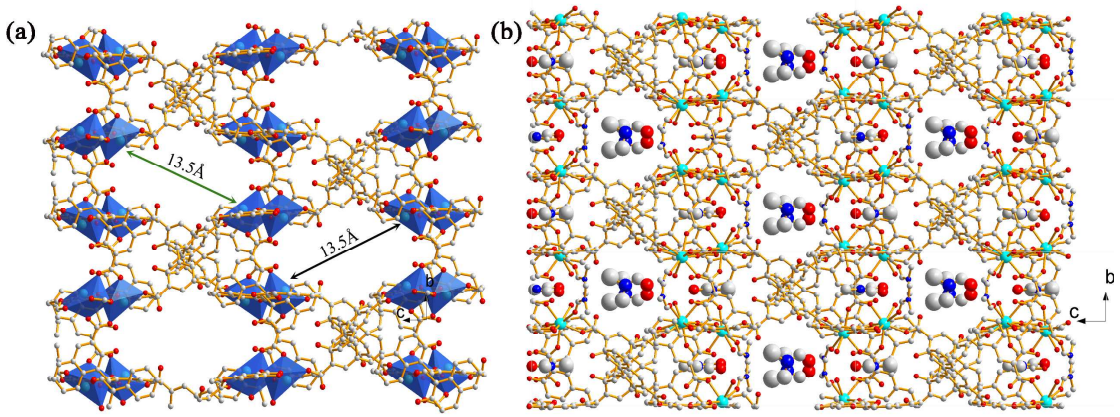

Fig. 8 (a) 3D porous structure of compound **2** along the *a* axis. (b) Representations of the DMF molecules filled in the pores of **2** with the DMF molecules represented with a space-filling model.

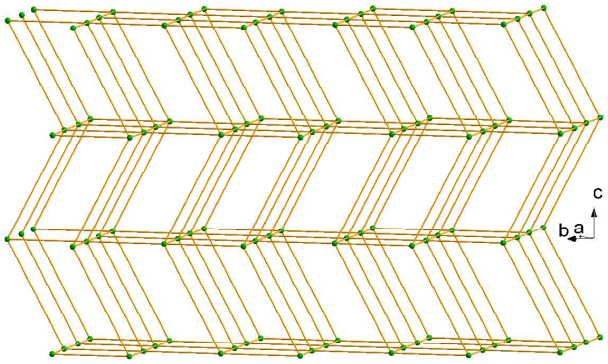

Fig. 9 Schematic topological view of the 3D structure of $\{4^{12}\cdot6^3\}$ topology in **2**. (Color code: $[Dy_2(COO)_6(DMF)_2(H_2O)_2]$, green ball; PA^{2-} anion, yellow line.)

PXRD and thermal stability

To confirm the phase purity of complexes **1** and **2**, the PXRD patterns were recorded at room temperature. As shown in Fig. S1-S2 (ESI†), the peak positions of the experimental PXRD patterns are in good agreement with the simulated data based on single-crystal diffraction results, demonstrating the high phase purity of all complexes.

Thermogravimetric analysis (TGA) was carried out to check the thermal stability of the compounds (Fig. S3, ESI†). For compound **1**, the TGA curve shows a gradual weight loss of 8.91% in the temperature range of 30-245 °C, corresponding to the loss of one lattice water and two lattice DMF molecules (calcd 9.25%). The following weight losses (7.58%), which end at ~ 320 °C, are attributed to the release of one coordinated DMF and three coordinated water molecules (calcd 7.16%). The framework starts to decompose after 320 °C. For compound **2**, the initial weight losses of 11.89% in the temperature range of 30-220 °C are due to the elimination of one latice water and three lattice DMF molecules (calcd 12.46%). The following weight losses (9.34%), which end at ~ 328 °C, are attributed to the release of two coordinated water and two coordinated DMF molecules (calcd 9.57%). The framework starts to decompose after 330 °C.

Magnetic properties

Temperature-dependent magnetic susceptibility measurements for **1** and **2** have been carried out in an applied magnetic field of 1000 Oe in the temperature range 2–300 K. The obtained data for both the compounds are shown as $\chi_M T$ vs T plots in Fig. 10. At 300 K, the $\chi_M T$ values are 28.37 and 28.10 cm^3 K mol^{-1} for **1** and **2**, respectively, corresponding to the expected value of 28.34 cm^3 K mol^{-1} for two uncoupled Dy^{3+} ions ($^6H_{15/2}$ ground term, S = 5/2, L =5, g =4/3, χT =14.17 cm^3 K mol^{-1}). For **1**, the $\chi_M T$ values increased gradually to the value of 34.14 cm^3 K mol^{-1} with decreasing temperature to about 25 K. Upon further cooling, the $\chi_M T$ values begin to decrease and reach 31.94 cm^3 K mol^{-1} at 2 K. Such behavior indicates the onset of weak ferromagnetic interactions between adjacent Dy^{3+} ions below 100 K.[39] Similar behaviors can also be observed in the reported Ln-MOFs (Ln = Dy,

Tb, Ho and Gd).[4a, 16b, 39] As for **2**, the $\chi_M T$ values decrease slowly then sharply to reach 22.96 cm^3 K mol^{-1} at 2 K. Such low temperature decrease of the $\chi_M T$ product could be ascribed to thermal depopulation of the Stark levels of the Dy(III) ions and/or the weak antiferromagnetic interactions between the spin carriers.[16-18] The field dependence of the magnetization for compounds **1** and **2** were collected at 2, 3, 4 and 5 K (Fig. S4). The magnetization at 7 T reaches 11.32 $N\mu_B$ for compound **1** and 12.03 $N\mu_B$ for compound **2** at 2 K (Fig. 11), respectively. The lack of true saturation in magnetization of the compounds suggests the presence of magnetic anisotropy and/or population of low lying excited states.[4b, 15, 17] It is further confirmed by the *M vs. H/T* plots where the isofield lines do not superimpose on a single master-curve as expected for an isotropic system with a well-defined ground state (Fig. S4).[17c]

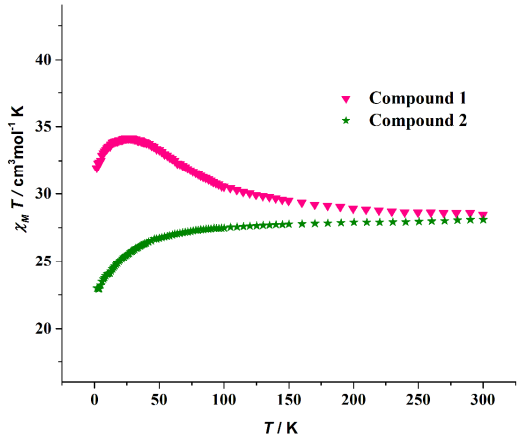

Fig. 10 Temperature dependence of $\chi_M T$ for **1** and **2** at 1 KOe between 2 and 300 K.

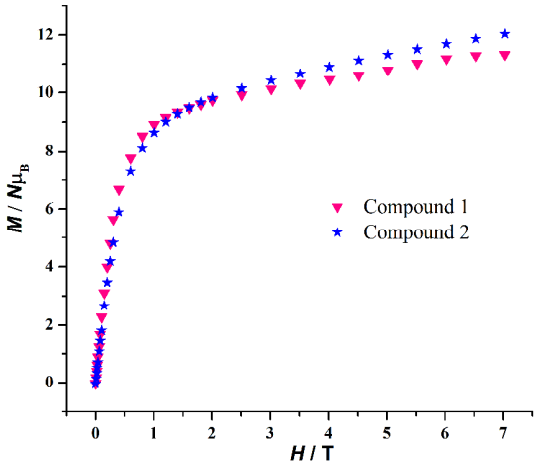

Fig. 11 Field dependence of the magnetization for **1** and **2** at 2K.

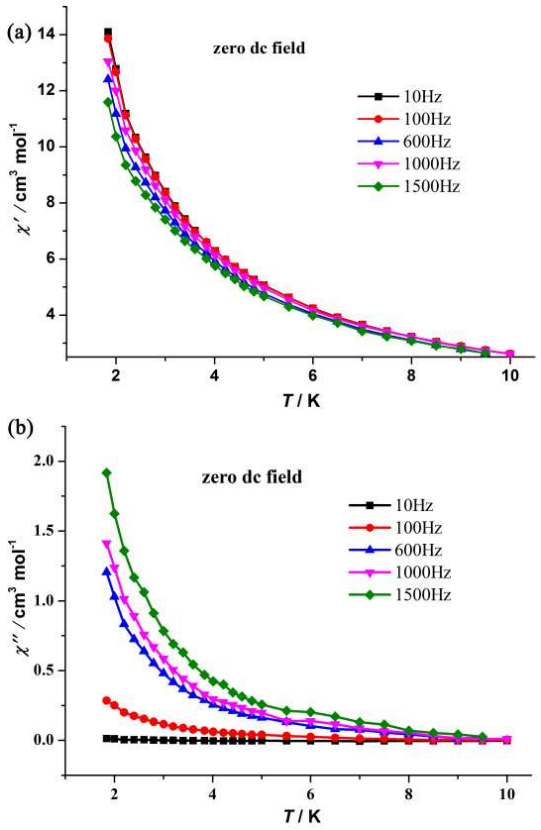

Fig. 12 Temperature dependence of the in-phase (χ′) and out-of-phase (χ″) ac susceptibility for **1**.

The dynamics of the magnetization of compounds **1** and **2** were investigated using alternating-current (ac) susceptibility measurements in the zero dc field. Both in-phase (χ′) and out-of-phase (χ″) components of ac susceptibility showed frequency dependence in compound **1** (Fig. 12). The frequency-dependent out-of-phase χ″ tails of signals at temperatures below ~10 K indicating the slow magnetization relaxation of an SMM with a small energy barrier for magnetization reversal. Such behavior most likely arises from predominant single-ion effects of the individual Dy^{3+} Kramer ions within **1**.[18a, b] Unfortunately, the maximum of χ″ signals were not observed above 2 K as the result of the fast quantum tunneling effects. Based on the assumption that a single relaxation process exists in **1**, the energy barrier and relaxation time can be roughly estimated from fitting the ac susceptibility by adopting the Debye model and equation, $\ln(\chi''/\chi') = \ln(\omega\tau_0) + Ea/k_BT$, yielding the energy barrier $Ea/k_B \approx 2.16$ K and the relaxation time $\tau_0 \approx 8.8 \times 10^{-6}$ s (Fig. 13), consistent

with the expected τ_0 values for an SMM.[33-36] This method is recently developed by Bartolomé *et al*, and has been applied in many compounds. [18] As for **2**, both in-phase (χ') and out-of-phase (χ'') signals are very weak, hardly showing frequency dependence (Fig. 14).

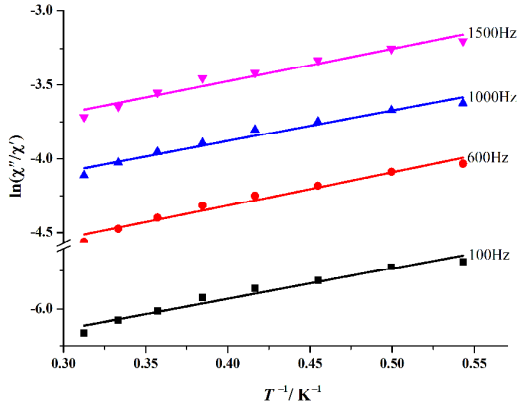

Fig. 13 Plots of ln(χ''/χ') vs T^{-1} for **1**; the solid line represents the fitting in the range of 1.8−4 K.

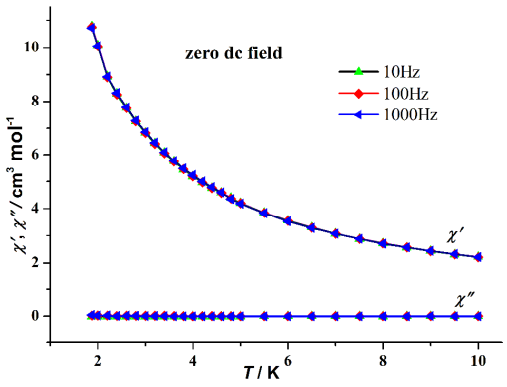

Fig. 14 Temperature dependence of the in-phase (χ') and out-of-phase (χ'') ac susceptibility for **2**.

Magneto-structural correlation studies

The magnetic exchange system in Ln-MOFs is very intricate in nature, and the SMM behaviour has proven to be governed by the interplay between the ligand field effect, coordination geometry and the strength of the magnetic interactions between the lanthanide sites. [19b,c] Recently, it has been increasingly identified that the observation of SMM properties in most lanthanide complexes is inherently related to the ligand field of the isolated lanthanide ion, [19-23] and effects of even subtle ligand field perturbations have shown to be of crucial importance in the observation of magnetization slow dynamics.[24-26] It is necessary to analyze the geometry exactly because the local anisotropy of the magnetic ion is strongly affected by the coordination geometry of the metallic center. The program SHAPE 2.1 was used to analyze the coordination geometries of the Dy^{3+} ions.[40] Table S2 reveals that the coordination geometries of Dy1 in **1** and Dy2 in **2** are closest to the triangular dodecahedron (D_{2d}), while that of Dy2 in **1** and Dy1 in **2** are very similar to the bicapped trigonal prism (C_{2v}), all of which are with some deviations. However, further analysis of Table S1-2 can find apparent differences in the coordination geometries around Dy^{3+} ions in **1** and **2**. The Dy–O bond distances around Dy1 and Dy2 in **1** are in the range of 2.286(2)–2.488(2) and 2.314(2)–2.476(3) Å, while that of the Dy^{3+} ions in **2** are in the range of 2.343(3)–2.454(3) and 2.269(3)–2.676(3) Å, respectively. In addition, the intra-molecular Dy···Dy distance of **2** (4.0045(1) Å) is slightly shorter than that in **1** (4.3721(0) Å), and the shortest Dy···Dy distance between adjacent SBUs is 6.6805(1) Å for **1**, while that in **2** is 11.3725(1) Å, possibly ruling out interactions between adjacent SBUs in **2**. [2b, 9b] Murugesu and co-workers have reported that minute differences in Dy–O bond lengths can result in clear changes to the local anisotropy of the Dy^{3+} ions and lead to distinct magnetic behaviors in a dinuclear system. [9b] We speculate that it is the differences in the local coordination sphere of each Dy^{3+} ions that leads to the distinct magnetic behaviors in **1** and **2**.

Luminescence properties

The UV−vis absorption spectra of the free ligand and complexes **1** and **2** are measured in dimethylformamide (DMF) solution ($c = 1 \times 10^{-5}$ mol/cm^3) and are displayed in Fig. 15. The absorption bands of H_2PA located in the region 275−290 nm can be primarily attributed to the π–π^* electronic transitions of the ligand. The broad lower energy transition is associated with the shift of electron density from the phenolate oxygen to the π^* orbital of the aromatic rings with a maximum at about 350 nm. The complexation with lanthanide does not have a significant influence on the singlet excited state

of the ligand. As expected, the absorption profiles of **1** and **2** are dominated by the ligand with the bands slightly red-shifted. Upon excitation at 365 nm (the lower energy absorption bands), the free ligand H_2PA features a broad emission band with the maximum at 472 nm (Fig. 16a). However, the solid-state photoluminescent spectra of complexes **1** and **2** display the typical bands of Dy^{3+} upon excitation at 365 nm. As shown in Fig. 16b, the two main bands of **1** and **2** are situated at 483, 575 nm and 485, 578 nm, respectively, which can be ascribed to the $^4F_{9/2} \rightarrow {}^6H_{15/2}$ and $^4F_{9/2} \rightarrow {}^6H_{13/2}$ transitions. The $^4F_{9/2} \rightarrow {}^6H_{13/2}$ transition is assigned to a hypersensitive transition with $\Delta J = 2$, which is extremely sensitive to the nature and symmetry of the coordinating environment of Dy^{3+} ion. It is well-known that luminescences from trivalent lanthanide ions arise from electronic transitions between the 4f orbitals, which are forbidden on symmetry grounds. There are usually two general approaches for attaining good luminescence. The first involves the addition of an organic ligand with strong light harvesting for efficient sensitizing the Dy^{3+} ion through intramolecular energy transfer. The second approach is to reduce the non-radiation processes of the centre ion's excited state by protecting the ion from high energy O–H oscillators. [38] Consequently, the little stronger emission intensity of compound **2** than that of compound **1** is reasonable in considering the fact that compound **1** contains three coordinated water molecules, while compound **2** has two.

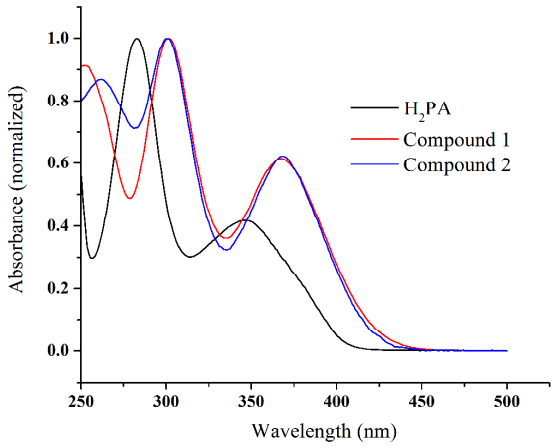

Fig. 15 UV−vis absorption spectra of the ligand and the corresponding compounds.

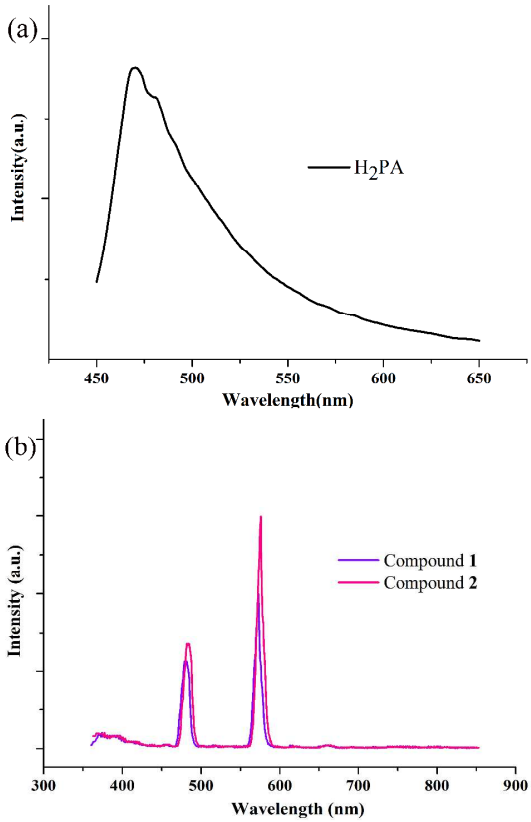

Fig. 16 Solid-state emission spectra of the ligand (a) and the corresponding compounds (b) (λ_{ex} = 365 nm).

Conclusions

In summary, we report here the pH-dependent synthesis, structures, magnetic and luminescent properties of two unprecedented dinuclear Dy-MOFs. Interestingly, both the complexes were obtained simultaneously within the pH range of 5.0-6.2, while higher pH values promote the formation of compound **1**, and lower pH values prefer to produce pure complex **2**. The slight structure difference in compounds **1** and **2** results in distinct magnetic properties. Compound **1** demonstrates a ferromagnetic interaction and slow magnetic relaxation behavior which is typical of single-molecule magnets, while antiferromagnetic interaction and no out-of-phase alternating-current signal were observed in compound **2**. Furthermore, both **1** and **2** exhibit characteristic luminescence of Dy^{3+} with different intensities upon excitation at 365 nm, which could find application as a potential light-emitting material. Our present findings will further enrich the crystal engineering strategy and

may be helpful to the rational design and assembly of novel Ln-MOFs with interesting magnetic and luminescent properties.

Acknowledgements

This work was supported by the National Natural Science Foundation of China (21371154).

†Electronic supplementary information (ESI) available: Selected bond lengths and angles, PXRD patterns, TGA curves for complexes **1** and **2**. For ESI and crystallographic data in CIF or other electronic format see DOI: 10.1039/xxxxxxxx

References

1 (*a*) L. Ungur, S. Y. Lin, J. Tang and L. F. Chibotaru, *Chem. Soc. Rev*., 2014, **43**, 6894; (*b*) P. Zhang, Y. N. Guo, J. Tang, *Coord. Chem. Rev*., 2013, **257**, 1728; (*c*) Y. N. Guo, G. F. Xu, Y. Guo, J. Tang, *Dalton Trans*., 2011, **40**, 9953; (*d*) S. Y. Lin, J. Tang, *Polyhedron*, 2014, **83**, 185; (*e*) M. Yamanouchi, D. Chiba, F. Matsukura, H. Ohno, *Nature*, 2004, **428**, 539; (*f*) L. Bogani, W. Wernsdorfer, *Nat. Mater*, 2008, **7**, 179; (*g*) G. E. Kostakis, A. M. Akoab, A. K. Powell, *Chem. Soc. Rev.*, 2010, **39**, 2238.

2 (*a*) Y.-N. Guo, G.-F. Xu, P. Gamez, L. Zhao, S.-Y. Lin, R. Deng, J. Tang, and H.-J. Zhang, *J. Am. Chem. Soc.*, 2010, **132**, 8538; (*b*) Y.-N. Guo, G.-F. Xu, W. Wernsdorfer, L. Ungur, Y. Guo, J. Tang, H.-J. Zhang, L. F. Chibotaru, A. K. Powell, *J. Am. Chem. Soc*., 2011, **133**, 11948; (*c*) S.-Y. Lin, W. Wernsdorfer, L. Ungur, A. K. Powell, Y. N. Guo, J. Tang, L. Zhao, L. F. Chibotaru and H.-J. Zhang, *Angew. Chem., Int. Ed.*, 2012, **51**, 12767; (*d*) P. Zhang, L. Zhang, C. Wang, S. Xue, S.-Y. Lin, J. Tang, *J. Am. Chem. Soc*., 2014, **136**, 4484; (*e*) Y.-N. Guo, L. Ungur, G. E. Granroth, A. K. Powell, C. Wu, S. E. Nagler, J. Tang, L. F. Chibotaru, D. Cui, *Sci. Rep*., 2014, **4**, 5471; (*f*) R. Sessoli, A. K. Powell, *Coord. Chem. Rev.*, 2009, **253**, 2328; (*g*) S. D. Jiang, B. W. Wang, G. Su, Z. M. Wang, S. Gao, *Angew. Chem*., *Int. Ed*., 2010, **122**, 7610; (*h*) J. D. Rinehart, M. Fang, W. J. Evans and J. R. Long, *Nat. Chem*., 2011, **3**, 538.

3 (*a*) N. Ishikawa, M. Sugita, W. Wernsdorfer, *Angew. Chem., Int. Ed*., 2005, **44**, 2931; (*b*) H. Wernsdorfer, K. Wang, J. Tao, J. Jiang, *Chem. Commun*., 2012, **24**, 2973; (*c*) J. J. LeRoy, M. Jeletic, S. I. Gorelsky, I. Korobkov, L. Ungur, L. F. Chibotaru, M. Murugesu, *J. Am. Chem. Soc*., 2013, **135**, 3502.

4 (*a*) Y. M. Song, F. Luo, M. B. Luo, Z. W. Liao, G. M. Sun, X. Z. Tian,Y. Zhu, Z. J. Yuan, S. J. Liu, W. Y. Xu and X. F. Feng, *Chem. Commun.*, 2012, **48**, 1006; (*b*) Q. Zhou, F. Yang, B. J. Xin, G. Zeng, X. J. Zhou, K. Liu, D. X. Ma, G. H. Li, Z. Shi and S. H. Feng, *Chem. Commun.*, 2013, **49**, 8244.

5 Y. X. Wang, W. Shi, H. Li, Y. Song, L. Fang, Y. Lan, A. K. Powell, W. Wernsdorfer, L. Ungur, L. F. Chibotaru, M. Shen, P. Cheng, *Chem. Sci*., 2012, **3**, 3366.

6 G. F. Xu, Q. L. Wang, P. Gamez, Y. Ma, R. Clérac, J. K. Tang, S. P. Yan, P. Cheng and D. Z. Liao, *Chem. Commun*., 2010, **46**, 1506.

7 Y. Z. Zheng, Y. H. Lan, W. Wernsdorfer, C. E. Anson, and A. K. Powell, *Chem. Eur. J*. 2009, **15**, 12566.

8 (*a*) L. Liang, G. Peng, G. Z. Li, Y. H. Lan, A. K. Powell and H. Deng, *Dalton Trans*., 2012, **41**, 5816; (*b*) M. Ren, S. S Bao, N. Hoshino, T. Akutagawa, B. W. Wang, Y. C. Ding, S. Q Wei, L. M. Zheng, *Chem. Eur. J*., 2013, **19**, 9619.

9 (*a*) M. E. Boulon, G. Cucinotta, J. Luzon, C. D. Innocenti, M. Perfetti, K. Bernot, G. Calvez, A. Caneschi, and R. Sessoli, *Angew. Chem. Int. Ed.*, 2013, **52**, 350. (*b*) F. Habib, J. Long, P.-H. Lin, I. Korobkov L. Ungur, W. Wernsdorfer, L. F. Chibotaruc and M. Murugesu, *Chem. Sci.*, 2012, **3**, 2158.

10 (*a*) M. Ren, S. S Bao, N. Hoshino, T. Akutagawa, B. W. Wang, Y. C. Ding, S. Q Wei, L. M. Zheng, *Chem. Eur. J*., 2013, **19**, 9619; (*b*) J. D. Rinehart, J. R. Long, *Chem. Sci*., 2011, **2**, 2078; (*c*) R. J. Blagg, C. A. Muryn, E. J. L. McInnes, F. Tuna, R. E. P. Winpenny, *Angew. Chem*., 2011, **123**, 6660; *Angew. Chem. Int. Ed*., 2011, **50**, 6530.

11 (*a*) P. H. Lin, T. J. Burchell, R. Clérac, M. Murugesu, *Angew. Chem*., 2008, **120**, 8980; (*b*) P. H. Lin, T. J. Burchell, L. Ungur, L. F. Chibotaru, W. Wernsdorfer, M. Murugesu, *Angew. Chem.*, 2009, **121**, 9653; (*c*) S. Demir, J. M. Zadrozny, M. Nippe, J. R. Long, *J. Am. Chem. Soc*., 2012, **134**, 18546.

12 (*a*) K. Suzuke, R. Sato and N. Mizuno, *Chem. Sci.*, 2013, **4**, 596; (*b*) G. Cucinotta, M. Perfetti, J. Luzon, M. Etienne, P. E.

Car, A. Caneschi, G. Calvez, K. Bernot, R. Sessoli, *Angew. Chem*., 2012, **124**, 1638.

13 X. N. Cheng, W. X. Zhang and X. M. Chen, *J. Am. Chem. Soc*., 2007, **129**, 15738.

14 (*a*) H. S. Ke, G. F. Xu, Y. N. Guo, P. Gamez, C. M. Beavers, S. J. Teat and J. Tang, *Chem. Commun*., 2010, **46**, 6057; (*b*) Z. L. Wang, W. H. Fang and G. Y. Yang, *Chem. Commun*., 2010, **46**, 8216.

15 F. Habib, J. Long, P. H. Lin, I. Korobkov, L. Ungur, W. Wernsdorfer, L. F. Chibotaru and M. Murugesu, *Chem. Sci*., 2012, **3**, 2158.

16 (*a*) Y. Wang, X. Li, T. W. Wang, Y. Song and X. Z. You, *Inorg. Chem.*, 2010, **49**, 969; (*b*) Ji. Xu, J. W. Cheng, W. P. Su and M. C. Hong, *Cryst. Growth Des*., 2011, **11**, 2294.

17 (*a*) J. Tang, I. Hewitt, N. T. Madhu, G. Chastanet, W. Wernsdorfer, C. E. Anson, C. Benelli, R. Sessoli and A. K. Powell, *Angew. Chem., Int. Ed.,* 2006, **45**, 1729; (*b*) S. Osa, T. Kido, N. Matsumoto, N. Re, A. Pochaba and J. Mrozinski, *J. Am. Chem. Soc*., 2004, **126**, 420; (*c*) P.-H. Lin, W.-B. Sun, M.-F. Yu, G.-M. Li, P.-F. Yan and M. Murugesu, *Chem. Commun*., 2011, **47**, 10993.

18 (*a*) D. I. Alexandropoulos, A. Fournet, L. C. Silva, A. M. Mowson, V. Bekiari, G. Christou, T. C. Stamatatos, *Inorg. Chem.*, 2014, **53**, 5420; (*b*) E. C. Mazarakioti, K. M. Poole, L. Cunha-Silva, G. Christoub and T. C. Stamatatos, *Dalton Trans*., 2014, **43**, 11456; (*c*) J. Bartolomé, G. Filoti, V. Kuncser, G. Schinteie, V. Mereacre, C. E. Anson, A. K. Powell, D. Prodius, C. Turta, *Phys. Rev. B*, 2009, **80**, 14430; (*d*) S. Y. Lin, G. F. Xu, L. Zhao, Y. N. Guo, Y. Guo, J. K. Tang, *Dalton Trans*., 2011, **40**, 8213; (*e*) P. F. Shi, Z. Chen, G. Xiong, B. Shen, J. Z. Sun, P. Cheng and B. Zhao, *Cryst. Growth Des*., 2012, **12**, 5203.

19 (*a*) N. F. Chilton, D. Collison, E. J. McInnes, R. E. Winpenny and A. Soncini, *Nat. Commun.*, 2013, **4**, 2551; (*b*) J. Long, F. Habib, P. H. Lin, I. Korobkov, G. Enright, L. Ungur, W. Wernsdorfer, L. F. Chibotaru and M. Murugesu, *J. Am. Chem. Soc*., 2011, **133**, 5319; (*c*) L. F. Zou, L. Zhao, P. Chen,Y. N. Guo,Y. Guo,Y. H. Li and J. K. Tang. *Dalton Trans*., 2012, **41**, 2966.

20 D. Aravena and E. Ruiz, *Inorg. Chem*., 2013, **52**, 13770.

21 J. D. Rinehart and J. R. Long, *Chem. Sci*., 2011, **2**, 2078.

22 J. Luzon and R. Sessoli, *Dalton Trans.*, 2012, **41**, 13556.

23 L. F. Zou, L. Zhao, P. Chen, Y. N. Guo, Y. Guo, Y. H. Li, J. K. Tang, *Dalton Trans*., 2012, **41**,2966.

24 F. Habib, P. H. Lin, J. Long, I. Korobkov, W. Wernsdorfer and M. Murugesu, *J. Am. Chem. Soc*., 2011, **133**, 8830.

25 K. S. Pedersen, L. Ungur, M. Sigrist, A.Sundt, M. Schau-Magnussen, V. Vieru, H. Mutka, S. Rols, H. Weihe, O. Waldmann, L. Chibotaru, J. Bendix and J. Dreiser, *Chem. Sci.*, 2014, **5**, 1650.

26 K. S. Pedersen, J. B. and R. Clérac, *Chem. Commun.*, 2014, **50**, 4396.

27 (*a*) L. S. Long, *CrystEngComm*, 2010, **12**, 1354; (*b*) M. Tsaramyrsi, M. Kaliva, A. Salifoglou,C. P. Raptopoulou, A. Terzis,V. Tangoulis and J. Giapintzakis, *Inorg.Chem*., 2001, **40**, 5772; (*c*) S. Faulkner and B. P. Burton-Pye, *Chem. Commun*., 2005, 259.

28 (*a*) L. Pan, X. Y.Huang, J. Li, Y. G. Wu, N. W. Zheng, *Angew. Chem. Int. Ed.,* 2000, **39**, 527; (*b*) Z. Chen, B. Zhao, Y. Zhang, W. Shi, P. Cheng, *Cryst. Growth Des*., 2008. **8**, 2291; (*c*) Wang, P; Fan, R. Q.; Yang, Y. L.; Liu, X. R.; Xiao, P.; Li, X. Y.; Hasi, W.; Cao, W. W. *CrystEngComm*., 2013, **15**, 4489.

29 (*a*) P. Wang, R. Q. Fan, X. R. Liu, L. Y. Wang, Y. L. Yang, W. W. Cao, B. Yang, W. Hasi, Q. Su, Y. Mu, *CrystEngComm*., 2013, **15**, 1931; (*b*) M. J. Polinski, S. Wang, E. V. Alekseev, J. N. Cross, W. Depmeier, T. E. Albrecht-Schmitt, *Inorg. Chem*., 2012, **51**, 11541; (*c*) Y.-F. Liu, G.-F. Hou, Y.-H. Yu, P. F. Yan, G.-M. Li, J. S. Gao, *New J. Chem.*, 2014, **38**, 1328; (d) Y. F. Liu, G.-F. Hou, Y. H. Yu, P. F. Yan, J. Y. Li, G. M. Li, J. S. Gao, *Cryst. Growth Des*., 2013, **13**, 3816.

30 (*a*) Q. Shi, Y. T. Sun, L. Z. Sheng, K. F. Ma, M. L. Hu, X. G.Hu, S. M. Huang, *Cryst. Growth Des*., 2008, **8**, 3401; (*b*) S. N. Wang, R. R. Yun, Y. Q. Peng, Q. F. Zhang, J. Lu,; J. M. Dou, J. F. Bai, *Cryst. Growth Des*., 2012, **12** ,79.

31 S. Biswas, H. S. Jena, S. Goswami, S. Sanda and S. Konar, *Cryst. Growth Des.,* 2014, **14**, 1287.

32 (*a*) G. M. Sheldrick, SHELXS-97, Program for Crystal Structure Solution, University of Göttingen, Göttingen, Germany, 1997. (*b*) G. M. Sheldrick, SHELXL-97, Program for Crystal Structure Refinement, University of Göttingen, Gö ttingen, Germany, 1997.

33 (*a*) N. Ishikawa, M.Sugita, T. Ishikawa, S.-Y. Koshihara, Y. Kaizu *J. Am. Chem. Soc.* 2003, **125**, 8694; (*b*) J. D. Rinehart, M. Fang, W. J. Evans, J. R. Long, *Nat. Chem.*, 2011, **3**, 538; (c) F. Habib, M. Murugesu, *Chem. Soc. Rev.* 2013, **42**, 3278.

34 L. Jia, Q. Chen, Y. S. Meng, H. L. Sun and S. Gao, *Chem. Commun*., 2014, **50**, 6052.

35 S. D. Jiang, B. W. Wang, G.. Su, Z. M. Wang and S. Gao, *Angew. Chem. Int. Ed*., 2010, **49**, 7448.

36 Y. Bi, Y. N. Guo, L. Zhao, Y. Guo, S. Y. Lin, S. D. Jiang, J. K. Tang, B. W. Wang and S. Gao, *Chem. Eur. J*., 2011, **17**, 12476.

37 A. L. Spek, *J. Appl. Crystallogr.*, 2003, **36**, 7.

38 (*a*) R. E. Whan, G. A. Crosby, *J. Mol. Spectrosc.*, 1962, **8**, 315; (*b*) S. V. Eliseeva, J.-C. G. Bunzli, *Chem. Soc. Rev*., 2010, **39**, 189; (*c*) F. L. Zhang, Y. H. Hou, C. X. Du, Y. J. Wu, *Dalton Trans*., 2009, 7359.

39 M. Chen, E. C. Sanudo, E. Jimenez, S. M. Fang, C. S. Liu and M. Du, *Inorg. Chem*., 2014, **53**, 6708.

40 (*a*) J. L. Liu, Y.C. Chen, Y.Z. Zheng, W. Q. Lin, L. Ungur, W. Wernsdorfer, L. F. Chibotaru and M. L. Tong, *Chem. Sci*., 2013, **4**, 3310; (*b*) T. Han, W. Shi, Z. Niu, B. Na, and P. Cheng, *Chem. Eur. J.* 2013, **19**, 994.

Table of contents

Highly pH-dependent synthesis of two novel three-dimensional dysprosium complexes with interesting magnetic and luminescent properties

Lina Zhang, Shuting Lu, Chao Zhang, Chenxia Du, and Hongwei Hou

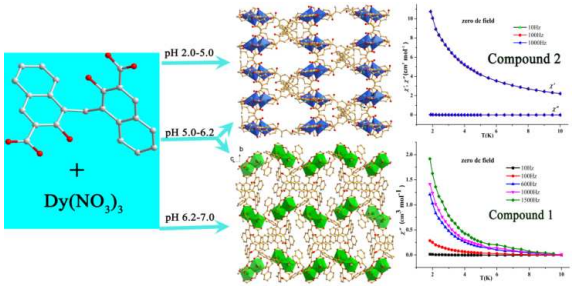

Two unprecedented Dy-MOFs with interesting magnetic and luminescent properties were obtained from identical starting materials and process with only different pH values.